A Numerical Solution for the Minimum Induced Drag of Nonplanar Wings

J. L. LUNDRY* AND P. B. S. LISSAMAN†
Douglas Aircraft Company, Long Beach, Calif.

A procedure has been developed for the accurate computation of the minimum induced drag of nonplanar wings with pylonlike panels, provided the wing front view consists of straight line segments. As is well known, the induced drag may be expressed as an integral in an auxiliary mapping plane. Previously, the main computational difficulty had been the determination of the Schwarz-Christoffel mapping between the real and the auxiliary planes. By means of the electrostatic analogy to potential flow, the constants of the mapping are determined with a small experimental error by using an analog field plotter. The mapping is then integrated by numerical techniques, and the constants are adjusted until the desired geometry is achieved to any order of accuracy. The induced drag is determined by quadrature and is shown by comparison with known test cases to be accurate to 10^{-4}. Comparison of results with earlier approximate solutions (Mangler, Cone) shows that some of the earlier approximate solutions give more favorable predictions (less drag) than the solution derived here. The discrepancies in the earlier work are shown to be due to improper boundary conditions, and some suggestions are made to minimize these effects. The results show a potential reduction of minimum induced drag of less than 1% for a current subsonic jet transport when the pylons are properly loaded.

Nomenclature

$A, \ldots, F$	=	potentials in the z plane
C_i	=	the ith condition
D_i	=	induced drag
E_0	=	electrical potential at the wing root
L	=	lift
U	=	freestream velocity
$a, \ldots, f$	=	potentials in the ζ plane
k	=	induced drag efficiency at minimum induced drag
l	=	fence length
p_j	=	jth independent variable
q	=	dynamic pressure
s	=	semispan
w_0	=	crossflow velocity
x, y	=	real and imaginary coordinates, respectively, in the z plane
z	=	complex variable
β	=	angle of loading inclination (Fig. 1)
ζ	=	complex variable
η	=	spanwise coordinate, $\eta = y/s$
ρ	=	density
φ	=	potential
φ_n	=	normal derivative of φ

Introduction

NONPLANAR lifting surfaces that produce minimum induced drag can be studied in three steps: 1) For a given configuration (wing alone, wing with end plates, etc.), determine the shed vorticity distribution to minimize induced drag for a specified lift. 2) Given 1, compute the minimum induced drag. 3) Given 1, compute the geometry (camber and/or twist) to produce the minimum induced drag loading. Mangler[1,2] studied the minimum induced drag of wings with end plates. His analytical treatment of 1 and 2 contains approximations that produce errors generally believed to be small.

To treat complex configurations, Cone[3] determined 1 experimentally, using the analogy between velocity potential and the electric potential in a medium of uniform conductivity. (Both potentials satisfy the Laplace equation.) Induced drag was then evaluated numerically.

Unfortunately, Mangler and Cone obtain induced drag efficiencies that differ significantly. For two configurations involving wings with end plates, Mangler attributes to the end plates increases of induced drag efficiency of 6 and 16% (relative to wing alone) while Cone's results are 14 and 22%, respectively. Both solutions contain approximations—Mangler's are analytical, Cone's are experimental.

The resolution of this discrepancy can be important to aircraft designers. Whereas end plates designed as such do not have overwhelming acceptance, portions of existing aircraft could be designed to obtain the benefits of end-plating. The pylons that suspend engines beneath wings are examples. Mangler's results indicate an increase of induced-drag efficiency of less than 1%, relative to wing alone, if the outboard pylon of a current subsonic jet transport is designed to minimize induced drag. If these results are correct, then aircraft designers should not concern themselves with minimizing the induced drag of the wing-pylon configuration, but should concentrate instead on minimizing the compressibility and viscous drag of the wing-pylon-nacelle combination, a formidable problem itself, with severe penalties for unfortunate design, as discussed in Ref. 4. On the other hand, Cone's method would give a significantly higher efficiency if the discrepancy mentioned previously is consistent. If the results of Ref. 3 are correct, the aircraft designer should consider the induced drag of the wing-pylon combination, greatly increasing the complexity of the wing-pylon-nacelle design problem, as discussed partially in Ref. 4, with an associated probable compromise in compressibility and viscous drag.

This paper presents a method of obtaining minimum induced drag in which the only errors (associated with quadratures) can theoretically be made as small as desired. The method is therefore effectively exact. The method is restricted to configurations with wake cross sections made up of straight line segments in order that the Schwarz-Christoffel transformation may be employed. Numerical results of this method are compared with those of Mangler and Cone. A partial explanation of the discrepancies is given.

Received April 17, 1967; revision received August 31, 1967. This paper summarizes work performed at the Aircraft Division under the sponsorship of the Independent Research and Development Program of Douglas Aircraft Company Inc.

* Engineer/Scientist Specialist, Aircraft Division.

† Consultant, Aircraft Division; also, Assistant Professor of Aeronautics, California Institute of Technology, Pasadena, Calif. Member AIAA.

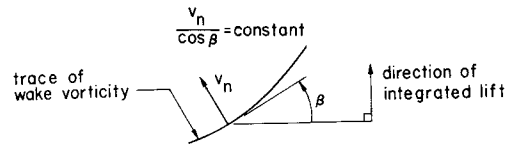

Fig. 1 Munk's minimum induced drag criterion.

Analysis

Munk[4] developed a procedure to determine the loading on an arbitrary configuration to produce minimum induced drag. All loadings are assumed light so that velocity perturbations are small, and the wake in the Trefftz plane may be assumed undistorted. The loadings are projected on a plane normal to the freestream velocity. This does not change the induced drag (Stagger Theorem). Munk's minimum induced drag criterion states that the induced velocity normal to the projected loadings must be proportional to the cosine of the angle of lateral inclination of the loadings. This criterion is illustrated in Fig. 1. He further demonstrates that the loading to satisfy this criterion can be found by solving a potential flow problem about the wake in the Trefftz plane, in which the undisturbed flow is parallel to the downwash. The desired loading is locally proportional to the potential difference across the wake and is normal to the wake.

Figure 2 shows the wake of a wing with an inboard fence that, in practice, might be an engine pylon. This configuration is used to demonstrate the procedure to determine minimum induced drag exactly. The potential in the z plane is required. This may be calculated by mapping the configuration into a line in an auxiliary ζ plane. The potential in the auxiliary ζ plane is readily written down, but the mapping, specified by its constants, a, b, c, d, e, and f, is undetermined. The Schwarz-Christoffel transformation between the planes is

$$\frac{dz}{d\zeta} = \frac{(\zeta - c)(\zeta - e)}{[(\zeta - a)(\zeta - b)(\zeta - d)(\zeta - f)]^{1/2}} \tag{1}$$

Given the geometry in the ζ plane, the geometry in the z plane is obtained by integrating Eq. (1). For example,

$$z_B - z_A = \int_a^b \frac{dz}{d\zeta}\, d\zeta \tag{2}$$

Each of the geometry integrals has either one or two integrable singularities. When an integral has two singularities, as in Eq. (2), it is evaluated in two parts of equal range. For example, one part of Eq. (2) has the form

$$\int_a^{\frac{1}{2}(a+b)} \frac{g(\zeta)}{(\zeta - a)^{1/2}}\, d\zeta = \int_a^{\frac{1}{2}(a+b)} \frac{g(\zeta) - g(a)}{(\zeta - a)^{1/2}}\, d\zeta + g(a) \int_a^{\frac{1}{2}(a+b)} \frac{d\zeta}{(\zeta - a)^{1/2}}$$

$$= \int_a^{\frac{1}{2}(a+b)} \frac{g(\zeta) - g(a)}{(\zeta - a)^{1/2}}\, d\zeta + 2g(a)\left[\frac{1}{2}(b - a)\right]^{1/2} \tag{2a}$$

If $g(\zeta)$ is expanded in a Taylor series about a, the last integrand becomes

$$(\zeta - a)^{-1/2}\{(\zeta - a)g'(a) + [(\zeta - a)^2/2]g''(a) + \ldots\}$$

As $g(a)$ contains no factors of the form $\zeta - a$, its derivatives are finite at $\zeta = a$, and the integrand goes to zero as $\zeta \to a$. The integral of Eq. (2a) can therefore be evaluated numerically. A modified Simpson rule is used with 49 intervals that are smaller near the singularity. Each of the geometry integrals can be analyzed by this procedure, once the constants of the mapping are known.

In the example of Fig. 2, the mapping derivative contains six unknown constants. Five of these constants are independent and determine the five lengths $\overline{AB}$, . . ., $\overline{EF}$ in the real plane. An iterative scheme is used to evaluate these constants. In this scheme, the geometry in the real plane is calculated by numerical integration in the auxiliary plane. Since the integrand and the limits of integration contain the unknown constants, an iteration scheme is not practical unless a very good first approximation of the constants is used.

The first approximation is obtained by considering an electrostatic representation of the flowfield in the real plane, using an analog field plotter. Since it is assumed that the complex potential is conserved between the real and auxiliary planes, the potential is identical at corresponding points of the mapping. The first approximation of these constants can be obtained experimentally by direct measurement in the analog of the real plane. For practical reasons, the measured potentials are scaled linearly before they are used in the iteration scheme; this scaling changes only the absolute scale of the geometry in the real plane, and is equivalent to fixing one of the five independent mapping constants. The geometry in the real plane must meet the four remaining conditions, which are relative: 1) The fence must close ($\overline{BC} = \overline{CD}$). 2) The wing must close ($\overline{AB} + \overline{DE} = \overline{EF}$). 3) The fence must have the desired spanwise location η [$\overline{AB} = \eta(\overline{AB} + \overline{DE})$]. 4) The fence must have the proper length l/s [$\overline{BC} = (l/s)(\overline{AB} + \overline{DE})$].

A linear iteration scheme is used to vary four of the six constants so that the four required conditions are satisfied. The corrections to these constants, Δp_j, are computed from

$$-\Delta C_j = (\partial C_i/\partial p_j)\Delta p_j \tag{3}$$

where ΔC_i is the error in C_i, the appropriate geometry condition. The 4×4 correction matrix $\partial C_i/\partial p_j$ is evaluated approximately by perturbing p_j slightly, computing C_i, and calculating the derivatives as though C_i varied linearly with p_j. In the example, a, b, d, and f are selected arbitrarily from the six unknown potentials as the independent variables. This iteration scheme is simple, and, for properly chosen parameters, converges rapidly. For some configurations, the mapping constants selected initially as independent variables did not give convergence, and another set was chosen. However, convergence has been achieved for each of the configurations considered.

After the iteration scheme gives the desired geometry, the minimum induced drag is calculated in terms of the efficiency k from the induced drag equation

$$D_i = L^2/4\pi s^2 qk \tag{4}$$

In terms of the crossflow potential in the Trefftz plane,

$$L = \rho U \int \Delta\varphi\, dy \tag{5}$$

and

$$D_i = \frac{1}{2}\rho \int \varphi\varphi_n ds \tag{6}$$

the appropriate integrals being taken about the wake. Munk's criterion for minimum induced drag is

$$\varphi_n = w_0 \cos\beta \tag{7}$$

so the minimum induced drag efficiency becomes

$$k = \frac{1}{\pi s^2 w_0} \int \Delta\varphi\, dy \tag{8}$$

If the integration is transformed into the ζ plane,

$$k = \frac{1}{\pi s^2} I \int_a^f \zeta \frac{dz}{d\zeta}\, d\zeta \tag{9}$$

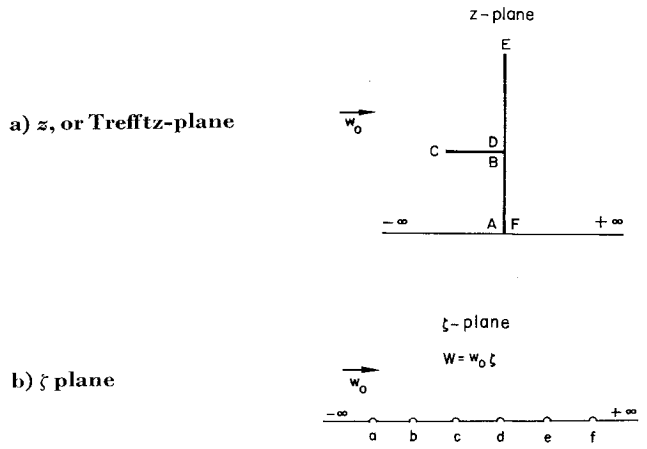

Fig. 2 Crossflow about symmetrical semispan wing with one fence.

where I means the "imaginary part of." The integral is evaluated numerically with the final values $a, \ldots, f$ and the semispan is given by

$$s = -\int_e^f \frac{dz}{d\zeta}\, d\zeta \tag{10}$$

The integrand of Eq. (9) contains integrable singularities that can be treated by the procedure used for the geometry integrals. The efficiency k determined by this procedure contains only errors of quadrature that are demonstrably small.

Results

Five Trefftz-plane configurations have been analyzed with the purpose of resolving the discrepancies between the results of Mangler and Cone, and of demonstrating the capability of the exact procedure. Figure 3 gives the efficiency of a wing with a single fence. In general, Mangler's values are quite close to the exact results. The two solutions for k from Ref. 3 are higher than the exact results by 9% and $5\frac{1}{2}$% for $\eta = 0.85$ and 1.0, respectively.

Figure 4 gives a second comparison of results of the three methods for a wing with end plates above and below. Mangler's results are given for plates of equal length, and are close to the exact solution. Cone's result is given for unequal plate lengths of 0.15 and 0.10 semispans. It is plotted in Fig. 4 at the average plate length and is compared directly with a single calculation by the exact method for the same configuration. One infers in this case that the unsymmetric

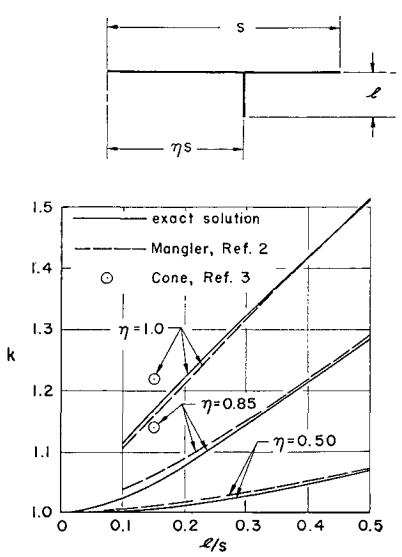

Fig. 3 Efficiency for minimum induced drag: semispan wing with one fence.

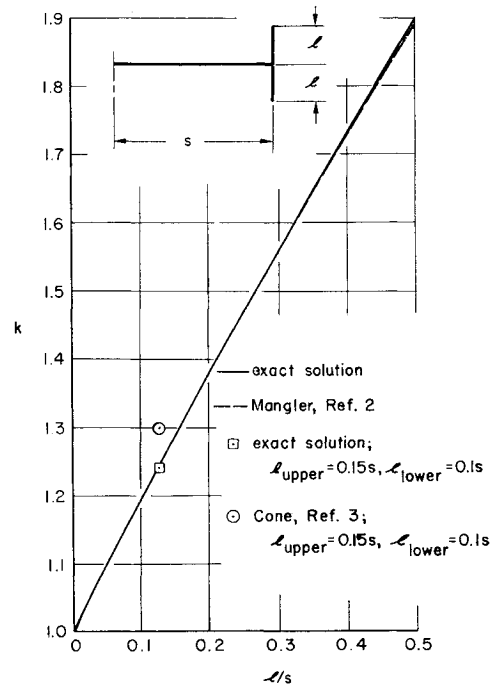

Fig. 4 Efficiency for minimum induced drag: semispan wing with end plates.

plates give essentially the same k as the symmetric plates of the same total length, and that the efficiency of Ref. 3 is too high by 6%.

Another comparison between the results of Mangler and of the exact solution is given in Fig. 5. The configuration is a generalization of the configuration of Fig. 3 to include arbitrary dihedral of the wing outboard of the fence. Mangler's result again agrees closely with the exact result.

A final comparison is made in Fig. 6. An approximate solution from Ref. 6 gives the efficiency for a biplane with minimum induced drag that agrees closely with the exact result. This example shows the increase of efficiency that could be obtained if the horizontal tail surface of a "T-tailed" aircraft carried the proper loading. The solution is academic as it ignores the load requirements usually imposed on the tail for equilibrium in pitch.

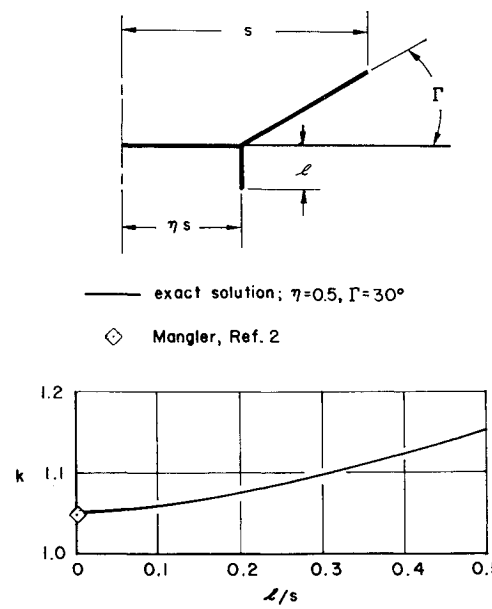

Fig. 5 Efficiency for minimum induced drag: semispan wing with inboard fence and dihedral outboard of fence.

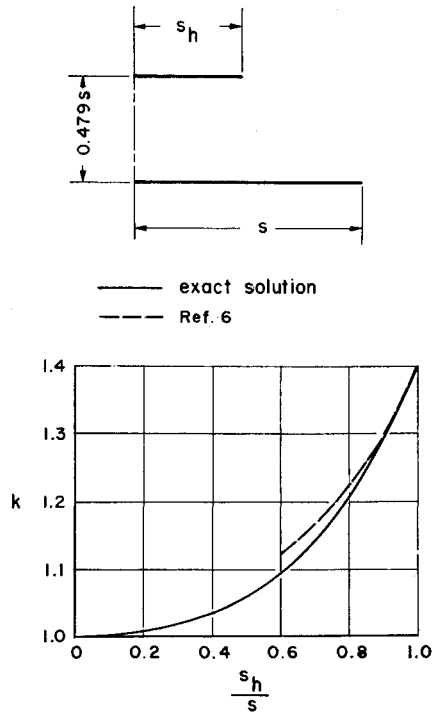

Fig. 6 Efficiency for minimum induced drag: biplane.

Figures 7 and 8 further demonstrate the capability of the present method (Fig. 4 is a special case of Fig. 8). The spanwise locations of the fences are those of the engine pylons on a current subsonic transport. These curves demonstrate that little increase of efficiency is possible, compared with wing alone, by proper loading of engine pylons for pylon lengths and locations typical of current transport aircraft.

The results of the exact method contain errors associated with numerical integration. To estimate the magnitude of these errors in k, the configurations of Figs. 3 and 5–8 were analyzed as monoplanes (the degenerate cases of $l = \Gamma = 0$). For these cases, the geometry conditions ΔC_i should be 0 and k should be 1.0. The results are given in Table 1.

Discussion of Results

From the evidence of Figs. 3–5, one concludes that Mangler's induced drag efficiencies are close to the exact results whereas Cone's values are significantly higher, and can have errors that exceed his estimated maximum error of 3%. The errors are caused in part by the use of a bounded potential field of finite size (the field plotter) instead of the infinite

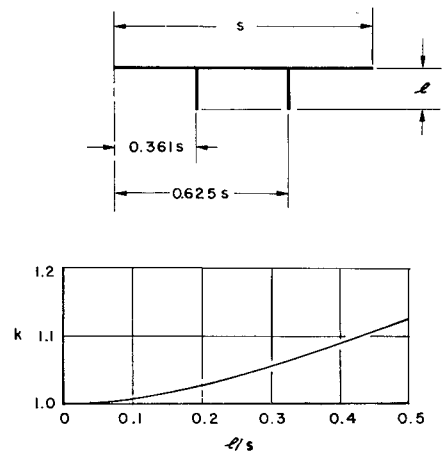

Fig. 7 Efficiency for minimum induced drag: semispan wing with two fences below.

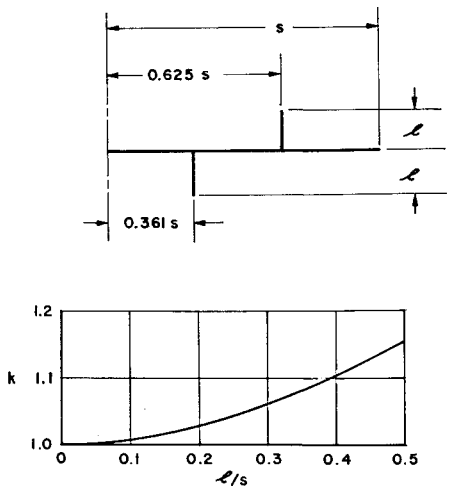

Fig. 8 Efficiency for minimum induced drag: semispan wing with one fence above and one fence below.

field required by theory. This type of error is commonly minimized by using a small wake model, relative to field size, but this approach in turn magnifies other types of errors. The analog experiment is usually performed with constant field size and constant potential difference between electrodes. As wake-model size is reduced, the potential differences across it are also reduced so that errors in potential measurements and errors caused by nonuniform conductivity in the field, which are independent of model size, become relatively larger. The choice of wake-model size is therefore a compromise. However, errors attributed to finite field size can serve a useful purpose. Reference 7 describes a method of estimating wind-tunnel wall effects by using an analog field shape geometrically similar to the wind-tunnel cross section.

Rheoelectric analog experiments have been used by Cone to simplify the process of obtaining theoretical aerodynamic results. In turn, aerodynamic theory can be used to reduce considerably the experimental errors caused by local field boundaries. Cone's expression for the analog of induced drag efficiency has the form

$$k = \frac{E_0}{(dE/dy)_\infty s} \int_{-1}^{1} \frac{E(\eta)}{E_0}\, d\eta \qquad (11)$$

The rectangular field boundaries commonly used when measuring $E(\eta)$ and $(dE/dy)_\infty$ produce errors in both. However, the theory of Ref. 6 (pp. 138–139) can be used to obtain field boundaries that are either equipotentials or streamlines in the crossflow about a monoplane. Examples of these

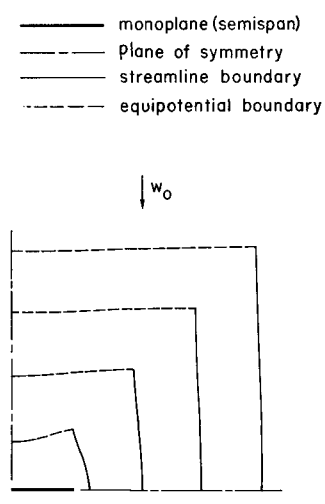

Fig. 9 Field boundaries that eliminate boundary distortion for crossflow about a monoplane.

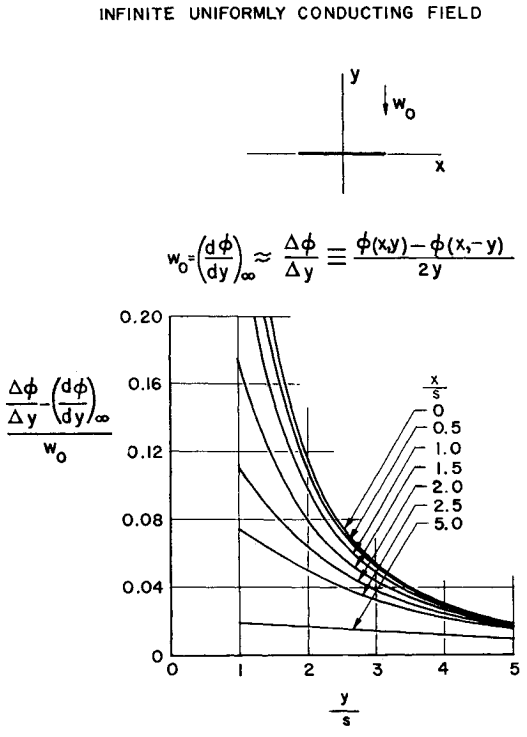

Fig. 10 Error in freestream crossflow velocity when measured near a monoplane.

field shapes are given in Fig. 9. These field boundaries will produce no errors in $E(\eta)/E_0$ for a monoplane.

The crossflow velocity $(dE/dy)_\infty$ is commonly approximated as $\Delta E/\Delta y$, where ΔE and Δy are the potential difference and distance, respectively, between the electrodes. The analytical monoplane crossflow can be used to compute the error in this procedure, given in Fig. 10, relative to hypothetical values for an infinite field. If the field boundaries of Fig. 9 are employed, Fig. 10 can be used to correct $\Delta E/\Delta y$ to $(dE/dy)_\infty$. The experimental value of k in Eq. (11) will then have no errors caused by boundary distortions for a monoplane, and considerably smaller boundary errors for other configurations. The experimental errors will then come chiefly from two sources—errors in measurement of E, ΔE, and Δy, and errors caused by nonuniform conductivity in the rheoelectric analog field.

Munk's criterion for minimum induced drag [Eq. (7)] requires vertical plates to carry a loading that eliminates local sidewash. Figure 11 gives isosidewash contours in the crossflow about a monoplane. One might guess that vertical plates located in regions of high sidewash might be more effective in reducing induced drag than vertical plates located elsewhere. This inference is substantiated by the results of Fig. 3.

Concluding Remarks

A numerical method has been developed for accurate computation of the minimum induced drag of nonplanar wings. The method is restricted to Trefftz-plane wake configurations composed of straight-line segments so that the Schwarz-

Table 1 Efficiencies for the monoplane degenerate cases

Configuration	Largest error $\lvert\Delta C_i\rvert$	k
Fig. 3	1×10^{-7}	0.99989
Fig. 5	3×10^{-6}	0.99992
Fig. 6	4×10^{-6}	1.00021
Fig. 7	4×10^{-5}	0.99984
Fig. 8	4×10^{-5}	0.99990

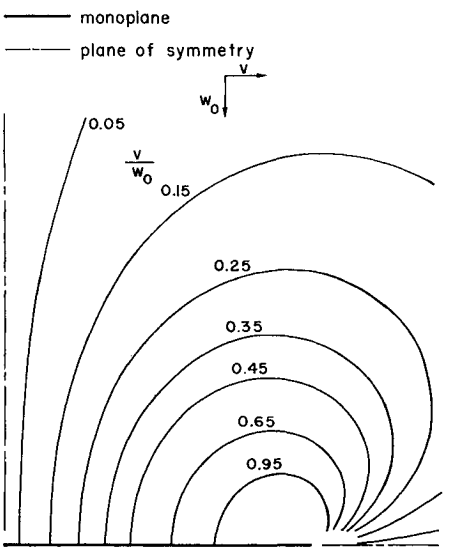

Fig. 11 Isosidewash lines in the crossflow about a monoplane.

Christoffel transformation can be used. Numerical results of the method show that Mangler's approximate analytical method gives accurate values of minimum induced drag. Cone's partially experimental method can produce significant errors; however, it remains the only method that can handle complex configurations. The experimental errors in Cone's method can be reduced by using the field shapes of Fig. 9 and by using Fig. 10 to correct experimental crossflow velocities as measured by Cone. The method presented here gives accurate results that serve as a standard of comparison for approximate solutions and is also of considerable value in that it can treat many significant configurations.

It is appropriate to repeat remarks by Cone about experiments involving fences. To obtain the induced drag efficiencies presented here, it is necessary that all surfaces support the proper loading, as described first in Ref. 5. In the past, some experiments have been performed using only plane fences (uncambered and untwisted) to serve as simple barriers to the crossflow, with disappointing results for k. These experiments were not very successful because, in general, the auxiliary surfaces as well as the main wing must be cambered and/or twisted to produce the proper loading.

References

[1] Mangler, W., "The lift distribution of wings with end plates," NACA TM 856 (1938); transl. by J. Vanier from "Die Auftriebsverteilung am Tragflügel mit Endscheiben," Luftfahrtforschung **14**, 564–569 (November 20, 1937).

[2] Mangler, W., "Lift distribution on wings with lateral plates," Douglas Aircraft Co. Rept. LB-33497 (December 1966); transl. by G. de Montalvo from "Die Auftriebsverteilung an Tragflügel mit seitlichen Scheiben," Luftfahrtforschung **16**, 219–228 (May 20, 1939).

[3] Cone, C. D., Jr., "The theory of induced lift and minimum induced drag of nonplanar lifting systems," NASA TR R-139 (1962).

[4] Kutney, J. T. and Piszkin, S. P., "Reduction of drag rise on the Convair 990 airplane," AIAA Paper 63–276 (1963).

[5] Munk, M. M., "The minimum induced drag of aerofoils," NACA Rept. 121 (1921).

[6] von Karman, T. and Burgers, J. M., "General aerodynamic theory—perfect fluids," *Aerodynamic Theory*, edited by W. F. Durand (Julius Springer-Verlag, Berlin/Vienna, 1934–36 and Dover Publications Inc., New York, 1963), Div. E, Vol. II, pp. 216–221.

[7] Malavard, L. C., "The use of rheoelectrical analogies in aerodynamics," AGARDograph 18 (August 1956).